Solid State Communications 252 (2017) 73–77

Contents lists available at ScienceDirect

Solid State Communications

journal homepage: www.elsevier.com/locate/ssc

Communication

Local atomic structure investigation of AlFeCuCrMg$_x$ (0.5, 1, 1.7) high entropy alloys: X-ray absorption spectroscopy study

Ornov Maulik[a], N. Patra[b], D. Bhattacharyya[b], S.N. Jha[b], Vinod Kumar[a,*]

[a] Department of Metallurgical and Materials Engineering, Malaviya National Institute of Technology, Jaipur 302017, India
[b] Atomic & Molecular Physics Division Bhabha Atomic Research Centre, Mumbai 400085, India

ARTICLE INFO

Keywords:
High entropy alloy
Mechanical alloying
X-Ray absorption spectroscopy
Immiscible alloys

ABSTRACT

The present paper reports local atomic structure investigation of novel AlFeCuCrMg$_x$ (x=0.5, 1, 1.7) high entropy alloys (HEAs) produced by mechanical alloying using Fe, Cr and Cu K-edge X-ray absorption near edge spectroscopy (XANES) and extended x-ray absorption fine structure (EXAFS) spectroscopy. XANES spectra measured at Fe and Cr K-edges resemble that of the respective pure metal foils, while the spectrum measured at Cu K-edge manifests the presence of some other phases in the as-milled alloys. The radial distribution functions (RDFs) obtained from Fourier transformation of EXAFS spectra support the formation of disordered BCC structure.

1. Introduction

High entropy alloys (HEAs) are the promising new era of alloy systems having remarkable properties which could lead to their potential usage in structural and automotive applications [1,2]. HEAs mainly consist of five or more elements in an equi-atomic or near equi-atomic concentrations with microstructures that may comprise to solid solution, intermetallic or amorphous phases [1–3]. Solid solutions of these multi-principal elements have been generally found to be more stable than intermetallic compounds because of their low enthalpy of mixing, high entropy of mixing and low atomic size difference of the constituent elements which bring down the Gibbs free energy of these systems and Hume-Rothery rules for alloy formation is satisfied [2]. Excellent properties in HEAs like very good thermal stability, high hardness, excellent corrosion resistance etc. are primarily because of the formation of such solid solutions which generally assume simple FCC and/or BCC structure [4]. The actual structure is however determined by the relative concentration (valence electron concentration) of FCC and BCC forming elements in the alloy.

However, it has been pointed out by various authors that the relative concentration of the structural phases present in the alloy system depends critically on the alloying process also [5]. Various techniques have been used for synthesis of HEAs like casting, mechanical alloying (MA), direct laser fabrication etc. MA is a powerful technique for the formation of metastable alloys between immiscible elements in equilibrium [6]. In the present manuscript we are mostly concerned with the structural studies and appearance of various phases in the alloy samples prepared by mechanical alloying (MA) process. Formation of alloys by MA between immiscible elements such as Fe–Cu, Ag–Fe, Cu–Cr, Cu-Co, Cu-V, Ag-Ni, Fe-Cr [6–11] has been studied in detail in the literature. Synthesis of high entropy alloys (HEAs) by MA technique was first reported by Varalakshmi et al. [12] and the resulting microstructure is found to be consisted of BCC solid solution.

Most of the reports in the literature have used diffraction studies to characterize the formation of solid solution in HEAs. However, diffraction studies cannot give a proper idea to the atomic level diffusion during MA because of the fact that the microstructure when coherent in nanometer level can have a single Bragg peak at the same lattice parameter [6,13]. Hence, it is essential and interesting to study the local atomic arrangement in the HEAs for better understanding of the alloy formation during MA and to predict potential lattice sites occupied by the atoms. X-ray absorption spectroscopy (XAS) which comprises of Extended X-ray absorption Fine Structure (EXAFS) and X-ray Near Edge Spectroscopy (XANES) techniques, is element specific and can extract information regarding the local structure around each elemental species separately apart from their oxidation states and a complete picture of the alloy system can be emerged from these complementary data. This is the main motivation for the present study. In the present experiment the elemental selectivity and short-range-order sensitivity of the XANES and EXAFS techniques have been used on synthesized AlFeCuCrMg$_x$ (x=0.5, 1, 1.7) HEAs [14] at Fe, Cr, Cu K-edge to study the local atomic structures around the probing atoms.

* Corresponding author.
E-mail address: vk.iitk@gmail.com (V. Kumar).

http://dx.doi.org/10.1016/j.ssc.2017.01.018
Received 2 September 2016; Received in revised form 28 November 2016; Accepted 17 January 2017
Available online 18 January 2017

2. Experimental details

The XANES and EXAFS measurement of the $AlFeCuCrMg_x$ (x=0.5, 1, 1.7) HEAs have been carried out at room temperature in the transmission mode at the Energy Scanning EXAFS beamline (BL-9) at INDUS-2 Synchrotron source (2.5 GeV, 100 mA), Raja Ramanna Center for Advanced Technology (RRCAT), Indore, India [15,16]. Three ionization chambers (300 mm length each) have been used for data collection in transmission mode, one ionization chamber for measuring incident flux (I_O), second one for measuring transmitted flux (I_t) and the third ionization chamber for measuring EXAFS spectrum of a reference metal foil for energy calibration. Proper gases with appropriate pressure were chosen to achieve 10–20% absorption in first ionization chamber and 70–90% absorption in second ionization chamber to obtain better signal to noise ratio. In order to obtain a proper edge jump the samples were taken in powder form of appropriate weight and were palletized to 15 mm diameter by mixing with 100 mg cellulose.

3. Results and discussion

3.1. Phase characterization

Detailed phase evolution in $AlFeCuCrMg_x$ (x=0.5, 1, 1.7) alloys during MA has been discussed elsewhere [14]. To give a brief account, the as-milled $AlFeCuCrMg_{0.5}$ HEA reveals BCC as the major phase and FCC as a minor phase while AlFeCuCrMg and $AlFeCuCrMg_{1.7}$ HEAs confirmed the formation of two BCC phases (BCC 1 and BCC 2). Stability of phase formed $AlFeCuCrMg_x$ (x=0.5, 1, 1.7) alloys was re-checked by XRD technique and were found to be intact. Usually, oxygen contamination is present in as- milled alloys because of milling environment or the milling medium used [17]. Oxygen contamination estimated using LECO analyzer were 0.32 wt%, 0.25 wt% and 0.014 wt % in as-milled $AlFeCuCrMg_{0.5}$, AlFeCuCrMg and $AlFeCuCrMg_{1.7}$ HEAs respectively [18].

3.2. Fe, Cr and Cu K-edge XANES

Fig. 1(a)–(c) show the normalized XANES spectra of the HEA samples along with that of standard metal foils measured at the Fe, Cr and Cu K-edges respectively. Fig. 1 indicates that the edge energies in the sample match with that of the respective metal foils confirming the elemental (0 oxidation) state of the metals in these alloy samples. Furthermore, the XANES spectra of the alloys at the Fe and Cr K-edges resemble that of the respective metal foils with two bumps in the edge energy region [19]. However, Cu K-edge XANES spectrum (Fig. 1(c)) of the samples, particularly of the low Mg alloy ($AlFeCuCrMg_{0.5}$), does not resemble with metallic Cu sample completely indicating the presence of some other phase in this sample.

3.3. Fe, Cr and Cu K-edge EXAFS

Fig. 2(a)–(c) show the normalized EXAFS ($\mu(E)$ versus E) spectra of the HEA samples measured at Fe and Cr and Cu K-edges respectively. The analyses of the EXAFS data have been carried out following the standard procedure [20,21] using the IFEFFIT software package [22]. This includes data reduction and Fourier transform to derive the $\chi(R)$ versus R plots from the absorption ($\mu(E)$ versus E) spectra, generation of the theoretical EXAFS spectra starting from an assumed crystallographic structure and finally fitting of the experimental $\chi(R)$ versus R data with the theoretical ones using the FEFF 6.0 code.

The experimental phase uncorrected $\chi(R)$ versus R plots of the samples at Fe, Cr and Cu K-edges have been shown in Fig. 3(a)–(c). The $\chi(R)$ versus R data for the respective metal foils are also shown in the above figures. Fig. 3(a) and (b) reveal that the $\chi(R)$ versus R plots of the samples at both the Fe and Cr K-edges are identical to each other due their nearby atomic numbers and similar crystal structure. It can also be seen that the plots at Fe and Cr K edges are identical to that of Fe and Cr metals. This further suggests that both Fe and Cr have the same kind of local structures as their metallic state and those do not change significantly with a change in Mg concentration in the HEAs. These results justify the formation of major BCC structures in the as-milled HEAs. The Fourier transformation of the EXAFS spectra to obtain the $\chi(R)$ versus R plots has been carried out using a window function in the k-range of 3–11 $Å^{-1}$ and the experimental spectra have been fitted with theoretically generated data in the R range of 1–5 Å for both Fe and Cr K-edge data.

XRD results of the samples show the presence BCC as a major phase in these HEAs [14]. Thus, in order to generate the theoretical $\chi(R)$ versus R plots BCC structure has been taken as input structure and various structural parameters have been obtained from ICSD database [23]. Though it is well known that for such high entropy alloy samples, each element has the same possibility to occupy the different lattice sites [2], to generate the theoretical EXAFS spectra we have assumed the BCC structure of 5-prinicipal element HEA alloy systems (of the type ABCDE) as shown in Fig. 4, where the body center position is occupied by Mg and all the remaining atoms are situated at the corner positions [2]. In this configuration, Mg atoms form the 1st coordination shell of the core absorbing atom (Fe or Cr) while the atoms sitting at corner positions form the 2nd and 3rd coordination spheres.

For fitting of the spectra, amplitudes of the scattering (NS_0^2) have been kept fixed for the different coordination shells for all the samples at a particular edge, while the bond distances and disorder (Debye-Waller) factors (σ^2), which give the mean-square fluctuations in the distances, have been varied during fitting. The goodness of the fit in the above process is generally expressed by the R_{factor} which is defined as:

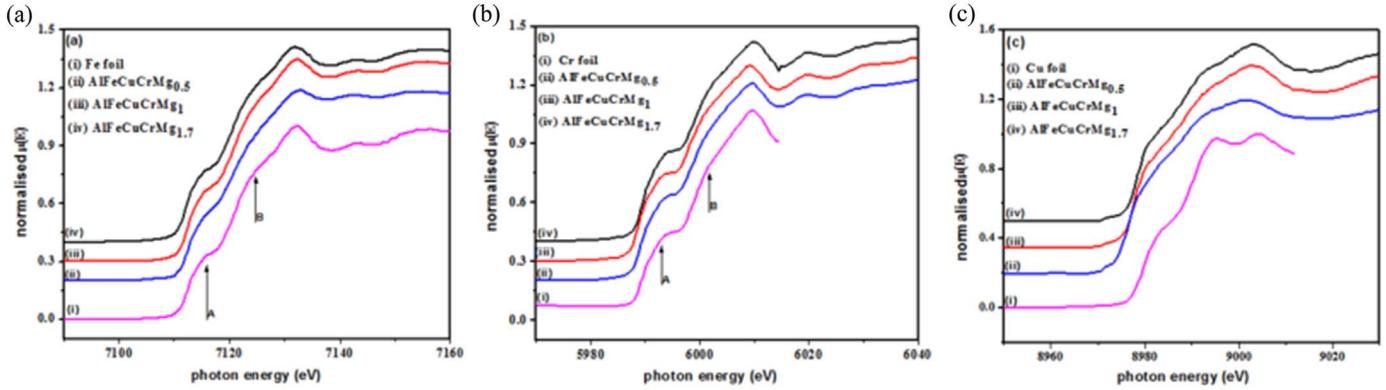

Fig. 1. Normalized XANES spectra of the HEAs at (a) Fe K-edge (b) Cr K-edge and (c) Cu K edge.

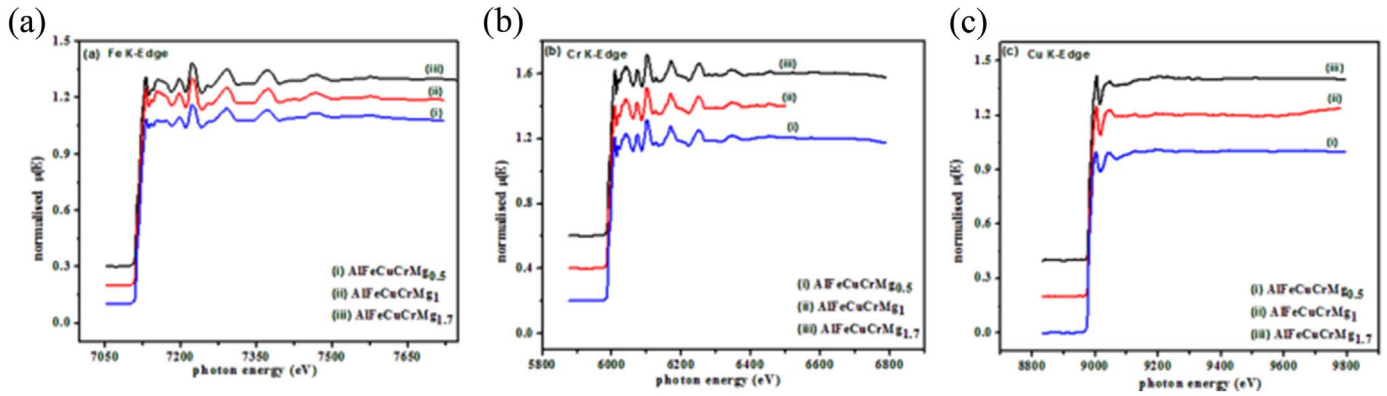

Fig. 2. Normalized EXAFS spectra of the HEAs at (a) Fe K-edge, (b) Cr K-edge and (c) Cu K-edge.

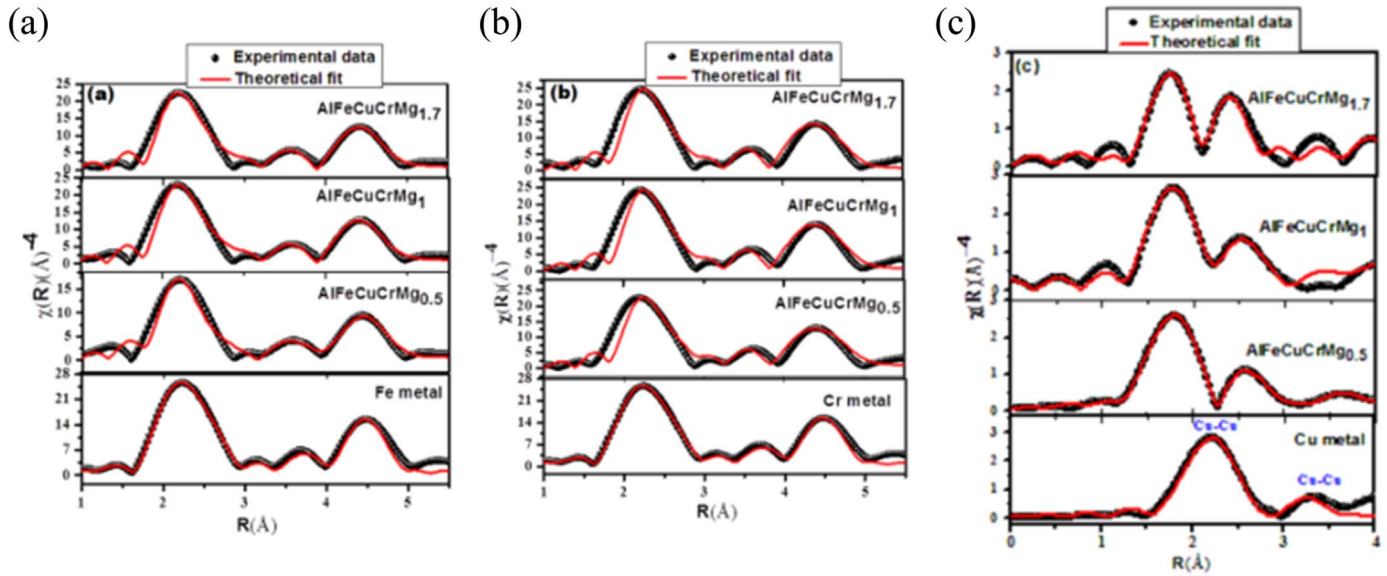

Fig. 3. Experimental $\chi(R)$ versus R plots along with the theoretical fitted plot of the HEAs samples at (a) Fe K-edge, (b) Cr K-edge and (c) Cu K-edge.

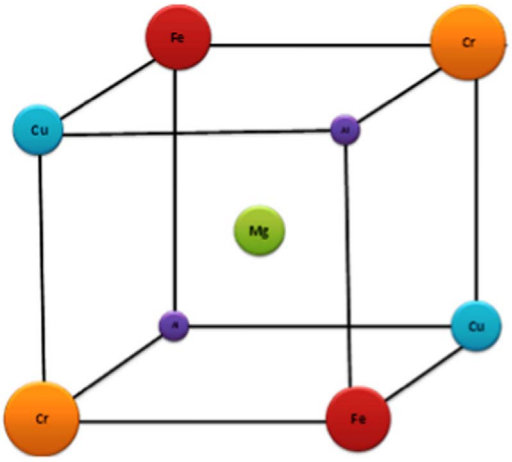

Fig. 4. Major BCC structure of the High Entropy Alloys (HEAs).

$$R_{factor} = \sum \frac{[\mathrm{Im}(\chi_{dat}(r_i) - \chi_{th}(r_i)]^2 + [\mathrm{Re}(\chi_{dat}(r_i) - \chi_{th}(r_i)]^2}{[\mathrm{Im}(\chi_{dat}(r_i)]^2 + [\mathrm{Re}(\chi_{dat}(r_i)]^2} \quad (1)$$

where, χ_{dat} and χ_{th} refer to the experimental and theoretical $\chi(R)$ values respectively and Im and Re refer to the imaginary and real parts of the respective quantities.

The best fit theoretical $\chi(R)$ versus R spectra of the samples are also shown in Fig. 3(a) and (b) along with the experimental data measured at Fe and Cr K edges and the values of the best fit parameters have been shown in Tables 1 and 2 respectively. Fe K-edge (Fig. 3(a)) data show three significant peaks in the $\chi(R)$ versus R plots, the 1st peak at ~2.2 Å appears little broader which is due to the contributions of 8 nearby Mg atoms at 2.48 Å in the 1st co-ordination shell and 2 Al, Cr and Cu atoms each at 2.87 Å in the 2nd co-ordination shell. The 2nd peak ~3.7 Å is due to the scattering from 12 Fe atoms at 4.06 Å in the 3rd co-ordination shell and the 3rd peak at ~4.5 Å appears due scattering from the 24 Fe and 8 Fe atoms at 4.76 Å and 4.97 Å respectively. Similar peaks appear also in the Cr K-edge $\chi(R)$ versus R plots (Fig. 3(b)) and the contributions of the different scattering paths in the respective peaks are also similar. The 1st peak is due to the mixed contributions of the nearby 8 Mg atoms at 2.49 Å and 2 Al, Fe and Cu atoms each at 2.88 Å. The 2nd peak arises due to scattering from 12 Cr atoms at 4.07 Å and the 3rd peak is due to 24 Cr and 8 Cr atoms at 4.78 Å and 4.99 Å respectively surrounding the core Cr atom. Fitting of the sample data suggests that the disorder in the structure increases with an increase in the Mg concentration in the samples which however also increases their entropy and stability. The overall structure of the sample however remains same over the whole concentration range of Mg.

Tables 1 and 2 reveal that for the alloy without Mg, the bond distance of the 1st co-ordination shell is very much close to the theoretical value. However, subsequent to inclusion of Mg to the lattice, the bond distance of the 1st coordination shell (viz., Fe-Mg or Cr-Mg) increases and remains almost same over the whole composition

Table 1
Structural parameters Fe K-edge.

Scattering paths	Parameters	Alloys		
		$AlFeCuCrMg_{0.5}$	$AlFeCuCrMg_1$	$AlFeCuCrMg_{1.7}$
Fe-Mg1(Fe)	R(Å) (2.485)	2.68 ± 0.01	2.67 ± 0.01	2.67 ± 0.01
	σ^2	0.004 ± 0.001	0.002 ± 0.001	0.002 ± 0.002
Fe-Al1	R(Å) (2.87)	2.71 ± 0.01	2.704 ± 001	2.703 ± 0.01
	σ^2	0.005 ± 0.004	0.004 ± 0.006	0.003 ± 0.003
Fe-Cr1	R(Å) (2.87)	2.71 ± 0.01	2.704 ± 0.01	2.703 ± 0.01
	σ^2	0.001 ± 0.001	0.001 ± 0.001	0.001 ± 0.001
Fe-Cu1	R(Å) (2.87)	2.71 ± 0.01	2.704 ± 0.01	2.703 ± 0.01
	σ^2	0.006 ± 0.006	0.002 ± 0.002	0.002 ± 0.002
Fe-Fe1	R(Å) (4.058)	3.96 ± 0.04	3.89 ± 0.04	3.89 ± 0.03
	σ^2	0.014 ± 0.023	0.011 ± 0.01	0.011 ± 0.01
Fe-Fe2	R(Å) (4.759)	4.95 ± 0.04	4.95 ± 0.04	4.95 ± 0.04
	σ^2	0.016 ± 0.008	0.015 ± 0.01	0.014 ± 0.01
Fe-Fe3	R(Å) (4.971)	4.96 ± 0.05	4.95 ± 0.02	4.95 ± 0.02
	σ^2	0.004 ± 0.003	0.002 ± 0.002	0.002 ± 0.003
	R_{factor}	0.009	0.006	0.004

Table 2
Structural parameters Cr K-edge.

Scattering paths	Parameters	Alloys		
		$AlFeCuCrMg_{0.5}$	$AlFeCuCrMg_1$	$AlFeCuCrMg_{1.7}$
Cr-Mg1(Cr)	R(Å) (2.494)	2.69 ± 0.01	2.69 ± 0.01	2.69 ± 0.01
	σ^2	0.007 ± 0.002	0.006 ± 0.002	0.006 ± 0.002
Cr-Al1	R(Å) (2.88)	2.74 ± 0.01	2.74 ± 0.01	2.74 ± 0.01
	σ^2	0.001 ± 0.004	0.002 ± 0.006	0.002 ± 0.007
Cr-Fe1	R(Å) (2.88)	2.74 ± 0.01	2.74 ± 0.01	2.74 ± 0.01
	σ^2	0.001 ± 0.001	0.001 ± 0.001	0.001 ± 0.002
Cr-Cu1	R(Å) (2.88)	2.74 ± 0.01	2.74 ± 0.01	2.74 ± 0.01
	σ^2	0.003 ± 0.002	0.002 ± 0.002	0.002 ± 0.002
Cr-Cr1	R(Å) (4.072)	3.99 ± 0.02	3.98 ± 0.011	4.01 ± 0.010
	σ^2	0.014 ± 0.015	0.014 ± 0.019	0.015 ± 0.011
Cr-Cr2	R(Å) (4.775)	4.69 ± 0.03	4.68 ± 0.03	4.69 ± 0.02
	σ^2	0.006 ± 0.004	0.005 ± 0.004	0.005 ± 0.004
Cr-Cr3	R(Å) (4.988)	5.07 ± 0.04	5.07 ± 0.04	5.04 ± 0.04
	σ^2	0.002 ± 0.006	0.002 ± 0.006	0.002 ± 0.006
	R_{factor}	0.025	0.019	0.015

range. This may be due to the smaller atomic radii of Mg (145 pm) than Fe (156 pm) and Cr (166 pm) [24]. This also causes the contraction of other coordination shells (Fe-Fe and Cr-Cr etc.) which is evident from Table 1. The above results justify the assumed models shown in Fig. 4.

3.4. Other phases in HEAs

Cu K-edge EXAFS (Fig. 3(c)) shows different results from the other two sets of data which reveals that the local structure around Cu atom is quite different from the Fe and Cr atoms in the high entropy alloy samples. As can be seen from Fig. 3(c), the phase uncorrected Cu K-edge spectrum shows a prominent peak around 1.7 Å is not present in the metallic Cu and hence has been attributed to some oxide phase present in the samples. Thus to generate the theoretical $\chi(R)$ versus R spectra for the Cu K-edge data a mixed phase of metallic Cu with the structure shown in Fig. 4 and CuO structure have been taken by giving them a weight factor of x% and (1-x) % respectively. In this case, the parameter x has also been varied along with bond length (R) and the Debye-Waller factor (σ^2) to fit the spectra. The Cu K-edge spectra are also characterized by the presence of three peaks. The 1st peak has mixed contributions of the Cu-O (CN=2) and Cu-Mg (CN=8) scattering paths at 1.95 Å and 2.49 Å respectively. The 2nd peak is due to scattering paths of Cu-Al, Cu-Cr and Cu-Fe (C.N=2 each) at 2.88 Å and the 3rd peak arises due to the Cu-Cu scattering paths (CN=12) at

Table 3
Structural parameters Cu K-edge.

Scattering paths	Parameters	Alloys		
		$AlFeCuCrMg_{0.5}$	$AlFeCuCrMg_1$	$AlFeCuCrMg_{1.7}$
Cu	x%	30.88	93.17	81.12
CuO	$_{(1-x)}$%	69.12	6.83	18.88
Cu-O1	R(Å) (1.951)	2.05 ± 0.01	2.16 ± 0.01	2.16 ± 0.01
	σ^2	0.005 ± 0.005	0.006 ± 0.002	0.003 ± 0.001
Cu-Mg1	R(Å) (2.494)	2.47 ± 0.01	2.35 ± 0.03	2.38 ± 0.01
	σ^2	0.028 ± 0.007	0.007 ± 0.004	0.013 ± 0.002
Cu-Al1	R(Å) (2.88)	2.97 ± 0.01	2.67 ± 0.05	2.95 ± 0.05
	σ^2	0.03 ± 0.001	0.03	0.001 ± 0.004
Cu-Cr1	R(Å) (2.88)	2.97 ± 0.01	2.67 ± 0.05	2.95 ± 0.05
	σ^2	0.019 ± 0.0003	0.001	0.028 ± 0.034
Cu-Fe1	R(Å) (2.88)	2.97 ± 0.01	2.67 ± 0.05	2.95 ± 0.05
	σ^2	0.021 ± 0.0003	0.001	0.023 ± 0.023
Cu-Cu1	R(Å) (4.07)	4.13 ± 0.01	3.94 ± 0.05	4.07 ± 0.04
	σ^2	0.03 ± 0.004	0.005 ± 0.006	0.016 ± 0.015
	R_{factor}	0.0001	0.006	0.008

4.07 Å. The best fit theoretical plots for the Cu K-edge have been shown in Fig. 3(c) along with the experimental data while the values of the best fit parameters have been given in Table 3.

In this case, the Cu-Mg bond length in the 1st co-ordination shell decreases with an increase in Mg concentration in the samples, whereas the Cu-O bond length increases. The variation of the Cu-Mg distance is found to be opposite to the variation of Fe-Mg and Cr-Mg distances with the increase in Mg concentration in the samples. This may be due to the fact that the calculated atomic radius of Mg is same as that of Cu (145 pm) and less than that of Fe and Cr [23]. However, the bond lengths of the 2nd and 3rd co-ordination shells do not show any regular variation with change in Mg concentration. Our earlier study [13] shows that $AlFeCuCrMg_{0.5}$ alloy contains some fraction of Cu type FCC phase which might have been oxidized to form CuO. Also, addition of higher amount of Mg increases the probability of formation of BCC structure and $AlFeCuCrMg_x$ (x=1, 1.7) HEAs thus lower fraction of CuO phase forms in these alloys. These results are also evident from XANES spectrum as shown in Fig. 1(c).

4. Conclusion

In summary, XANES and EXAFS measurements at Fe, Cu and Cr K edges have been used to study the local atomic structure of $AlFeCuCrMg_x$ (x=0.5, 1, 1.7) HEAs synthesized by MA. The bond length distribution determined from Fe and Cr K-edge EXAFS measurements can be interpreted in favor of the formation of majorly BCC phase however; Cu K-edge data have shown formation of some copper oxide phases in the alloys. The fraction of oxide phase is maximum in $AlFeCuCrMg_{0.5}$ alloy and substantially decreases for $AlFeCuCrMg_x$ (x=1, 1.7) HEAs.

Acknowledgement

Authors are thankful to DST-SERB no. SB/FTP/ETA-181/2013, New Delhi for financial assistance.

References

[1] B.S. Murty, J.W. Yeh, S. Ranganathan, High-Entropy Alloy, first ed., Elsevier Inc, London, 2014.
[2] Y. Zhang, T.T. Zuo, Z. Tang, M.C. Gao, K.A. Dahmen, P.K. Liaw, Z.P. Lu, Prog. Mater. Sci. 61 (2014) 1–93.
[3] M.H. Tsai, J.W. Yeh, Mater. Res. Lett. 2 (2014) 107–123.
[4] Y. Chen, Y. Hu, C. Tsai, C. Hsieh, S. Kao, J. Yeh, T. Chin, S. Chen, J. Alloy Comp. 477 (2009) 696–705.
[5] R. Sriharitha, B.S. Murty, R.S. Kottada, Intermetallics 32 (2013) 119–126.
[6] E. Ma, Prog. Mater. Sci. 50 (413) (2005) 413–509.
[7] K.B. Gerasimov, S.V. Mytnichenko, S.V. Pavlov, V.A. Chernov, S.G. Nikitenko, J. Alloy. Comp. 252 (1997) 179–183.
[8] J.H. He, H.W. Sheng, P.J. Schilling, C.-L. Chien, E. Ma, Phys. Rev. Lett. 86 (2001) 2826–2829.
[9] A. Froideval, R. Iglesias, M. Samaras, S. Schuppler, P. Nagel, D. Grolimund, M. Victoria, W. Hoffelner, Phys. Rev. Lett. 99 (2007) (237201-1-237201-237204).
[10] E. Ma, J.H. He, P.J. Schilling, Phys. Rev. B 55 (1997) 5542–5545.
[11] J.H. He, E. Ma, Phys. Rev. B 64 (2001) (144206-1-144206-12).
[12] S. Varalakshmi, M. Kamaraj, B.S. Murty, J. Alloy. Comp. 460 (2008) 253–257.
[13] J.H. He, H.W. Sheng, J.S. Lin, P.J. Schilling, R.C. Tittsworth, E. Ma, Phys. Rev. Lett. 89 (2002) (125507-1-125507-4).
[14] O. Maulik, V. Kumar, Mater. Charact. 110 (2015) 116–125.
[15] S. Basu, C. Nayak, A.K. Yadav, A. Agrawal, A.K. Poswal, D. Bhattacharyya, S.N. Jha, N.K. Sahoo, J. Phys.: Conf. Ser. 493 (2014) (012032-1-012032-012034).
[16] A.K. Poswal, A. Agrawal, A.K. Yadav, C. Nayak, S. Basu, S.R. Kane, C.K. Garg, D. Bhattachryya, S.N. Jha, N.K. Sahoo, AIP Conf. Proc. 1591 (2014) 649–651.
[17] C. Suryanarayan, Mechanical alloying and milling, Prog. Mater. Sci. 46 (2001) 1–184.
[18] O. Maulik, D. Kumar, S. Kumar, D.M. Fabijanic, V. Kumar, Intermetallics 77 (2016) 46–56.
[19] ⟨http://www.camd.lsu.edu/beamline_info/XrayInfo/Reference_X-Ray_Spectra_for_Metal_Foils.pdf⟩
[20] D.C. Konigsberger, R. Prince, X-Ray Absorption: Principles, Applications, Techniques of EXAFS, SEXAFS and XANES, first ed., Wiley, New York, 1988.
[21] S.D. Kelly, D. Hesterberg, B. Ravel, A.L. Ulery, L.R. Drees (Eds.), Analysis of Soils and Minerals Using X-ray Absorption Spectroscopy, Methods of Soil Analysis, Part 5–mineralogical Methods, Soil Science Society of America, Madison, WI, USA, 2008, pp. 367–464.
[22] M. Newville, B. Ravel, D. Haskel, J.J. Rehr, E.A. Stern, Y. Yacoby, Physica B208 (1995) 154–156.
[23] ⟨https://www.fiz-karlsruhe.de/icsd.html⟩.
[24] E. Clementi, D.L. Raimondi, W.P. Reinhardt, J. Chem. Phys. 47 (1967) 1300–1307.